The Experimental Determination of Interfacial Energies for Solid Zn in Equilibrium with Zn-Al-Sb Liquid

YEMLIHA ALTINTAS, ESRA ÖZTÜRK, SEZEN AKSÖZ, KAZIM KEŞLIOĞLU, and NECMETTIN MARAŞLI

The equilibrated grain boundary groove shapes of solid Zn in equilibrium with Zn-Al-Sb liquid were observed from a quenched sample using a radial heat flow apparatus. The Gibbs–Thomson coefficient, solid–liquid interfacial energy, and grain boundary energy of the solid Zn were determined from the observed grain boundary groove shapes. The thermal conductivity of the eutectic solid phase for Zn-0.4 at. pct Al-0.4 at. pct Sb alloy and the thermal conductivity ratio of the liquid phase to the solid phase for Zn-0.4 at. pct Al-0.4 at. pct Sb alloy at eutectic temperature were also measured with a radial heat flow apparatus and a Bridgman-type growth apparatus, respectively.

DOI: 10.1007/s11663-015-0393-z

I. INTRODUCTION

THE solid–liquid interfacial energy, σ_{SL}, is recognized to play a key role in a wide range of metallurgical and materials phenomena from wetting[1] and sintering through phase transformations and coarsening.[2] Thus, a quantitative knowledge of σ_{SL} values is necessary. However, the determination of σ_{SL} is difficult. Since 1985, a technique for the quantification of solid–liquid interfacial energy from the grain boundary groove shape has been used.[3–18] Observation of groove shape in a thermal gradient can be used to determine the interfacial energy, independent of the grain boundary energy because the interface near the groove must always satisfy

$$\Delta T_r = \left[\frac{1}{\Delta S*}\right]\left[\left(\sigma_{SL}+\frac{d^2\sigma_{SL}}{d\theta_1^2}\right)\kappa_1+\left(\sigma_{SL}+\frac{d^2\sigma_{SL}}{d\theta_2^2}\right)\kappa_2\right], \quad [1]$$

where ΔT_r is the curvature undercooling, ΔS^* is the entropy change per unit volume, θ_1 and θ_2 refer to the orientations of interfaces, and κ_1 and κ_2 are the mean curvatures of the interfaces. When the solid–liquid interfacial energy is isotropic, Eq. [1] becomes

$$\Delta T_r = \frac{\sigma_{SL}}{\Delta S^*}\left(\frac{1}{r_1}+\frac{1}{r_2}\right), \quad [2]$$

where r_1 and r_2 are the principal radii of the curvature of the surface. For the case of a planar grain boundary intersecting a planar solid–liquid interface, $r_2 = \infty$ and the Eq. [2] becomes

$$\Gamma = r\,\Delta T_r = \frac{\sigma_{SL}}{\Delta S^*}, \quad [3]$$

where Γ is the Gibbs–Thomson coefficient. This equation is called the Gibbs–Thomson relation.[13]

At present, the most powerful experimental method to measure solid–liquid interfacial energy is the grain boundary groove method. This method is based on the direct application of the Gibbs–Thomson equation and can be applied to measure σ_{SL} for multi-component systems as well as pure materials, for opaque materials as well as transparent materials, for any observed grain boundary groove shape, and for any value of the thermal conductivity ratio of the equilibrated liquid phase to solid phase, $R = K_L/K_S$, where K_S is the thermal conductivity of the solid phase and K_L is the thermal conductivity of the liquid phase.

The investigation of lead-free systems is important in order to be able to find a replacement for the existing lead-based alloys used mostly in electronic devices, as well as in other processes. The system investigated here is one of the selections made on the basis of the Zn-Al binary system. The main characteristic of this system is that until now it has no major applications, resulting mainly from the lack of experimental data. The investigation of such alloys, especially in the zinc-rich corner, is very difficult from the experimental point of view, even though the zinc-rich alloys in this system are

YEMLIHA ALTINTAS, Research Assistant, is with the Department of Materials Science and Nanotechnology, Faculty of Engineering, Abdullah Gül University, 38039 Kayseri, Turkey. ESRA ÖZTÜRK, Research Assistant, is with the Department of Physics, Faculty of Arts and Science, Kocaeli University, 41380 Kocaeli, Turkey. SEZEN AKSÖZ, Associate Professor, is with the Department of Physics, Faculty of Arts and Science, Nevşehir Hacı Bektaş Veli University, 50300, Nevşehir, Turkey. KAZIM KEŞLIOĞLU, Professor, is with the Department of Physics, Faculty of Science, Erciyes University, 38039, Kayseri, Turkey. Contact e-mail: kesli@erciyes.edu.tr NECMETTIN MARAŞLI, Professor, is with the Department of Metallurgical and Materials Engineering, Faculty of Chemical and Metallurgical Engineering, Yıldız Technical University, 34210, Davutpaşa-İstanbul, Turkey.

Manuscript submitted September 17, 2014.
Article published online June 16, 2015.

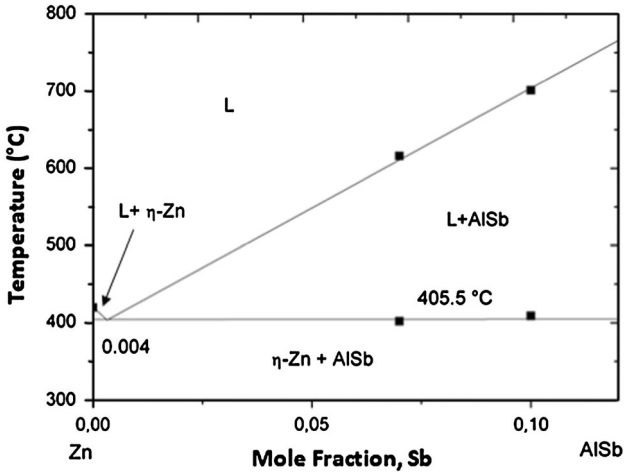

Fig. 1—The phase diagram of Zn-Al-Sb eutectic system.[19]

already in use for galvanizing processes.[19] A few studies on zinc coatings were made by Peng *et al.*[20] and Zhang.[21] Therefore, the Zn-Al-Sb ternary alloy has considerable potential for galvanizing processes.

Although the phase diagram of the Zn-Al-Sb ternary system has been determined,[19] as shown in Figure 1, some of its thermo-physical properties such as solid–liquid interfacial energy, Gibbs–Thomson coefficient, grain boundary energy, and thermal conductivity of the solid and liquid phases for Zn-Al-Sb ternary alloy have not as yet been fully determined. These thermo-physical properties could be used by those making comparisons between experimentally observed solidification morphology and predictions from theoretical models. Thus, the aim of the present work was to determine the thermal conductivity, Gibbs–Thomson coefficient, solid–liquid interfacial energy, and grain boundary energy for solid Zn in equilibrium with Zn-Al-Sb eutectic liquid.

II. MATERIALS AND METHODS

A. *Sample Production*

In order to observe the equilibrated grain boundary groove shapes in opaque materials, Gündüz and Hunt[13] designed a radial heat flow apparatus. Maraşlı and Hunt[14] improved the experimental apparatus for higher temperatures. The details of the apparatus and experimental procedures are given in References 13 through 17. In the present work, a similar apparatus was used to observe the grain boundary groove shapes in the Zn-Al-Sb eutectic system.

It is necessary to consider what happens during the annealing period. Consider a binary eutectic system. If the alloy composition (X_0) is near the eutectic composition ($X_0 \cong X_E$) above the eutectic temperature, a binary eutectic system consists of liquid. If this system is held in a very stable temperature gradient, there will be no liquid droplets behind the solid phases and two solid phases (α, β) can grow together on the eutectic structure.

In the present study, the composition of the alloy was chosen as Zn-0.4 at. pct Al-0.4 at. pct Sb to grow a single solid Zn phase on the eutectic cast structure in a short annealing time from the phase diagram of Zn-Al-Sb alloy.[19] Zn which has the highest composition in Zn-Al-Sb ternary alloy was placed into the graphite crucible. Then the graphite crucible was landed into the vacuum furnace using a wire. Since the melting temperature of Zn is 692.68 K (419.68 °C), the vacuum furnace was heated up to 800 K (527 °C) for 2 hours. Then Antimony and Aluminum, which have 903.78 K and 933.47 K (630.78 °C and 660.47 °C) melting temperatures, respectively, were dropped into the zinc melt in the graphite crucible. To obtain a homogeneous mixture, molten alloying elements were stirred with a graphite bar for two hours. The Zn-0.4 at. pct Al-0.4 at. pct Sb alloy was prepared in a vacuum furnace using 99.99 pct Zn, 99.9 pct Al, and 99.5 pct Sb. After the forming of ternary alloy, the molten alloy was poured into a graphite crucible as shown in Figure 2(c) held in a specially constructed casting furnace at approximately 50 K above the melting temperature of the alloy. The molten alloy was then directionally solidified from bottom to top to ensure that the crucible was completely full. The sample was then placed in the radial heat flow apparatus.

In the present work, the composition of ternary alloy was chosen as Zn-0.4 at. pct Al-0.4 at. pct Sb. The final composition of the Zn-Al-Sb ternary alloy after alloying process was determined using the EDX composition analysis. EDX result is illustrated in Figure 2. As can be seen in Figure 2, the final composition of Zn-Al-Sb ternary alloy is Zn-3.49 at. pct Al-3.43at. pct Sb and the loss of Zn is very limited. So the solid phase is still Zn.

The sample was heated from its center by a single heating wire as shown in Figure 3(b), and the outside of the sample was kept constant to an accuracy of ±0.01 K at 283 K (10 °C) using a *Poly Science digital 9102* model heating/refrigerating circulating bath to maintain a constant radial temperature gradient on the sample. A thin liquid layer (1 to 2 mm thick) was melted around the central heating wire, and the specimen was annealed in a very stable temperature gradient over a long period. During the annealing period, the liquid droplets move radially toward the hot zone of the sample by temperature gradient zone melting and the single solid phase can grow on the eutectic cast phase, as shown in Figure 4. If the temperature difference between solidus and liquidus lines is high, the freezing range will be larger and the equilibrating (annealing) time will be long. The equilibrating (annealing) time for Zn-0.4 at. pct Al-0.4 at. pct Sb alloy was 3 days. During the annealing period, the temperature in the specimen and the vertical temperature variations on the sample were continuously recorded by the stationary thermocouples and a moveable thermocouple, respectively, using a data logger *via* computer. The input power was also recorded periodically. The temperature in the sample was kept stable to about ±0.03 K for up to

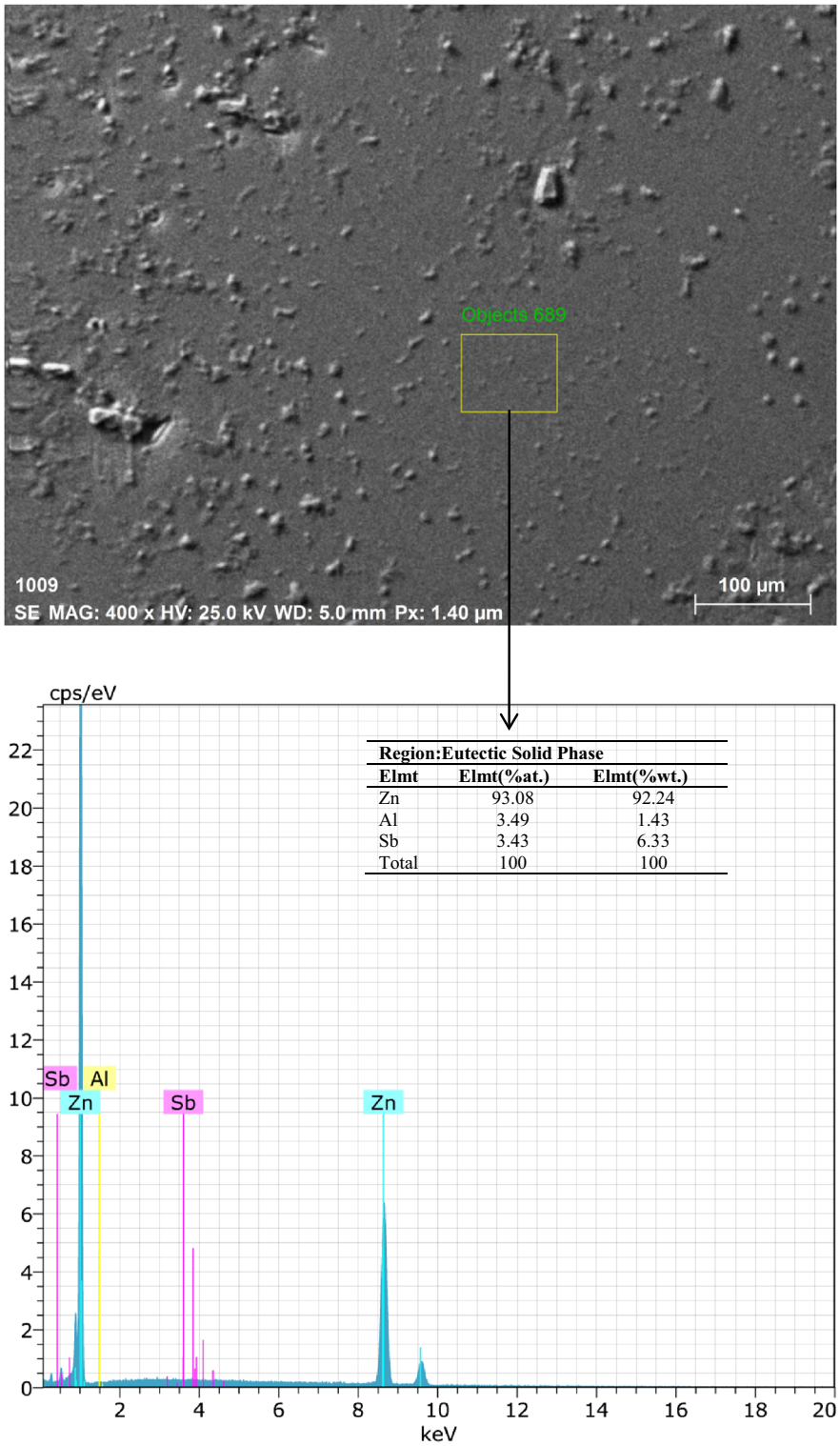

Fig. 2—The chemical composition analysis of the Zn-0.4 at. pct Al-0.4 at. pct Sb ternary eutectic alloy using SEM EDX.

3 days. At the end of the annealing time, the specimen was rapidly quenched by turning off the input power which was sufficient to get a well-defined solid–liquid interface, because the liquid layer around the central heating wire was very thin (typically less than 0.5 to 1 mm).

B. *Measurements of the Coordinates of Equilibrated Grain Boundary Groove Shapes*

The quenched sample was cut transversely into lengths of typically 25 mm, and transverse sections were ground flat with 180 grit SiC paper. Grinding and

polishing were then carried out by following a standard route. After polishing, the samples were etched in 100 mL water and hydrofluoric acid solution (90 mL water and 10 mL hydrofluoric acid) for 10 seconds.

The equilibrated grain boundary groove shapes were then photographed with an *Olympus DP12* type CCD digital camera placed on top of an *Olympus BX51* type light optical microscope. A graticule ($200 \times 0.01 = 2$ mm) was also photographed using the same objective. The photographs of the equilibrated grain boundary groove shapes and the graticule were superimposed on one another using *Adobe PhotoShop 8.0* version software, so that the accurate measurement of the groove coordinate points on the groove shapes could be made.

C. *Geometrical Correction for the Groove Coordinates*

The coordinates of the cusp, x, y, should be measured using the coordinates x, y, z where the x-axis is parallel to the solid–liquid interface, the y-axis is normal to the solid–liquid interface, and the z-axis lies at the base of the grain boundary groove. Maraşlı and Hunt[14] devised a geometrical method to make appropriate corrections to the groove shapes, and the details of the geometrical method are given in Reference 14.

The coordinates of the equilibrated grain boundary groove shapes were measured with an optical microscope, to an accuracy of ± 10 μm, by following Maraşlı and Hunt's geometrical method so that appropriate corrections to the shape of the grooves could be deduced.[14] The uncertainty in the measurements of the equilibrated grain boundary groove coordinates is 0.1 pct.

D. *Measurements of the Thermal Conductivity of Solid and Liquid Phases*

The thermal conductivity ratio of the equilibrated eutectic liquid phase (Zn-0.4 at. pct Al-0.4 at. pct Sb) to the solid Zn phase, $R = K_{\mathrm{L(eutectic\ liquid)}}/K_{\mathrm{S(Zn)}}$, must be known or measured to evaluate the Gibbs–Thomson coefficient with the present numerical method. The radial heat flow method is an ideal technique for measuring the thermal conductivity of the solid phase. The thermal conductivity of the solid Zn phase is also needed to evaluate the temperature gradient in the solid phase. In the radial heat flow method, a cylindrical sample (100 mm in length and 30 mm in diameter) was heated using a single heating wire in an alumina tube along the axis at the center of the sample, and the sample was kept in a temperature gradient for four hours to achieve a steady-state condition as shown in Figure 3. At the steady-state condition, the temperature gradient in the cylindrical specimen is given by Fourier's law:

$$G_{\mathrm{S}} = \frac{\mathrm{d}T}{\mathrm{d}r} = -\frac{Q}{2\pi r \ell K_{\mathrm{S}}}, \qquad [4]$$

where Q is the total input power, r is the distance of the solid–liquid interface to the center of the sample, ℓ is the length of the heating wire which is constant, and K_{S} is the thermal conductivity of the solid phase. Integration of Eq. [4] gives

$$K_{\mathrm{S}} = a_0 \frac{Q}{T_1 - T_2}, \qquad [5]$$

where

$$a_0 = ln(r_2 / r_1)/2\pi\ell, \qquad [6]$$

is an experimental constant, r_1 and r_2 ($r_2 > r_1$) are the fixed distances from the central axis of the specimen, and T_1 and T_2 are the temperatures at the fixed positions, r_1 and r_2, respectively, as shown Figure 3. Equation [5] could be used to obtain the thermal conductivity of the solid phase by measuring the difference in temperature between two fixed points for a given power level provided that the vertical temperature variation is minimum or zero.

The thermal conductivity of the eutectic solid (Zn-0.4 at. pct Al-0.4 at. pct Sb) was measured with the radial heat flow apparatus. Sufficient amounts of metallic materials were melted to produce an ingot of approximately 100 mm in length and 30 mm in diameter in a vacuum furnace using 99.99 pct Zn, 99.9 pct Al, and 99.5 pct Sb. After stirring, the molten metallic alloy was poured into a graphite crucible held in a specially constructed hot filling furnace at approximately 100 K above the melting temperature of the alloy. The molten metallic alloy was then directionally solidified from bottom to top to ensure that the crucible was completely full. The specimen was then placed in the radial heat flow apparatus.

The specimen was heated from the center using a single heating wire (140 to 190 mm in length and 2.5 mm in diameter, *Kanthal A–1*) in steps of 50 K up to 10 K below the melting temperature of the alloy, and the outside of the sample was cooled to an accuracy of $\pm$ 0.01 K at 283 K (10 °C) using a *Poly Science digital 9102* model heating/refrigerating circulating bath to maintain a constant radial temperature gradient on the sample. To obtain a reliable value of thermal conductivity in the thermal conductivity measurement, a larger radial temperature gradient is desired. For this purpose, the gap between the cooling jacket and the specimen was filled with graphite dust and the outside of the specimen was kept at 283 K (10 °C) using a heating/refrigerating circulating bath. The length of central heating wire was chosen as 10 mm longer than the length of specimen to make the isotherms parallel to the vertical axis. The specimen was kept at a steady-state condition for at least two hours at a constant temperature.

The input power is expressed as

$$Q = \frac{V_{\mathrm{sh}}}{R_{\mathrm{sh}}} V_{\mathrm{h}}, \qquad [7]$$

where V_{sh} and V_{h} are the potential differences between the ends of the shunt and the ends of the central heating wire, respectively, and R_{sh} is the shunt resistance. Since the current is too high (100 amps) on the heating wire, it is impossible to measure the current accurately

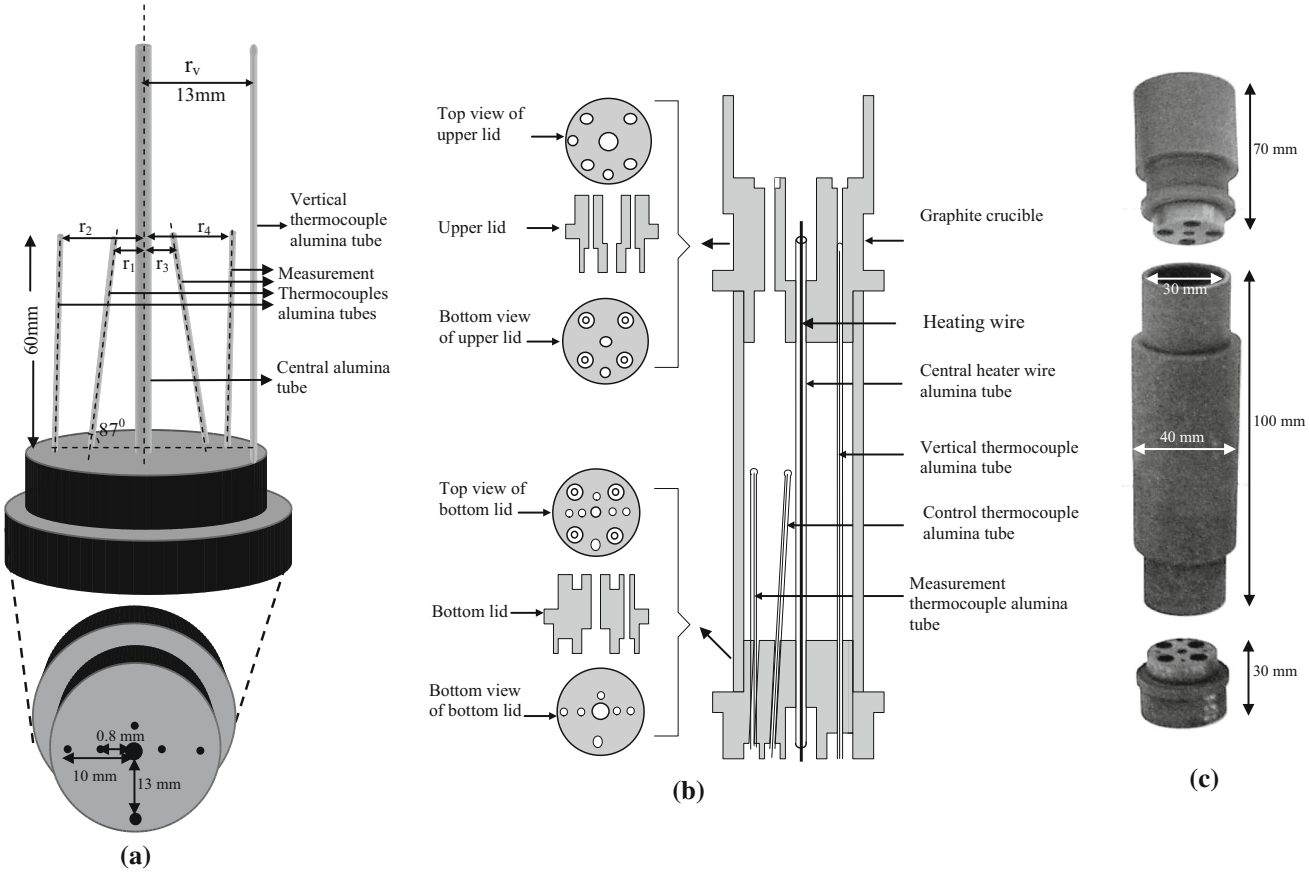

Fig. 3—(*a*) The positions of alumina tubes in graphite crucible. (*b*) Schematic illustration of graphite crucible. (*c*) Photograph of graphite crucible.

via a direct method. In order to measure the current on the heating wire, a shunt was constructed. Therefore, 30 Kanthal-1 wires (2.65 mm radius and 210 mm length) were connected in parallel on two drilled copper blocks. The connections were made by silver soldering. For a reliable power measurement, the resistance of the shunt had to be accurately measured using two digital multi-meters. The measurement of the shunt resistance gives 1.893×10^{-3} Ω. The potential differences between the ends of the shunt and ends of the heating wire could be measured to be 142.67×10^{-3} and 3.756 V, respectively. The total input power could be measured to be about 283.08 W using the very accurately measured shunt resistance and the potential differences between the ends of shunt and ends of the heating wire.

At steady state, the stationary thermocouple temperatures were recorded with a *Pico TC-08* data logger. The temperatures on the different parts of the specimen were measured with mineral-insulated, metal-sheathed, 0.5-mm-diameter, K-type thermocouples. A zero or minimum vertical temperature gradient is desired in thermal conductivity measurements. The vertical temperature for each setting was kept constant by moving the central heater up and down. After all desired power settings and temperature measurements had been completed during the heating procedure, the cooling procedure was started in the same steps down to room temperature.

Then the sample was removed from the furnace and cut transversely near to the measurement points; after that the specimen was ground and polished for the measurements of r_1 and r_2. The positions of the thermocouples were then photographed with an *Olympus DP12*CCD digital camera placed in conjunction with an *Olympus BX51* type light optical microscope. A graticule ($200 \times 0.01 = 2$ mm) was also photographed using the same objective. The photographs of the positions of the thermocouples and the graticule were superimposed on one another using *Adobe PhotoShop 8.0* software, so that the accurate measurement of the distances of the stationary thermocouples could be made to an accuracy of ±10 μm. The transverse and longitudinal sections of the specimen were examined for porosity, crack, and casting defects to make sure that these would not introduce any error in the measurements.

The thermal conductivity of the eutectic solid *vs* temperature is plotted in Figure 5. A comparison of the thermal conductivity of the eutectic solid with the thermal conductivities of Zn,[22] Al[23], and Sb[24] is also given in Figure 5. The value of K_S for the Zn-Al-Sb eutectic solid at the eutectic temperature was obtained to be 91.30 W/Km, by extrapolating the line to the eutectic temperature as shown in Figure 5.

It is not possible to measure the thermal conductivity of the liquid phase with the radial heat flow apparatus

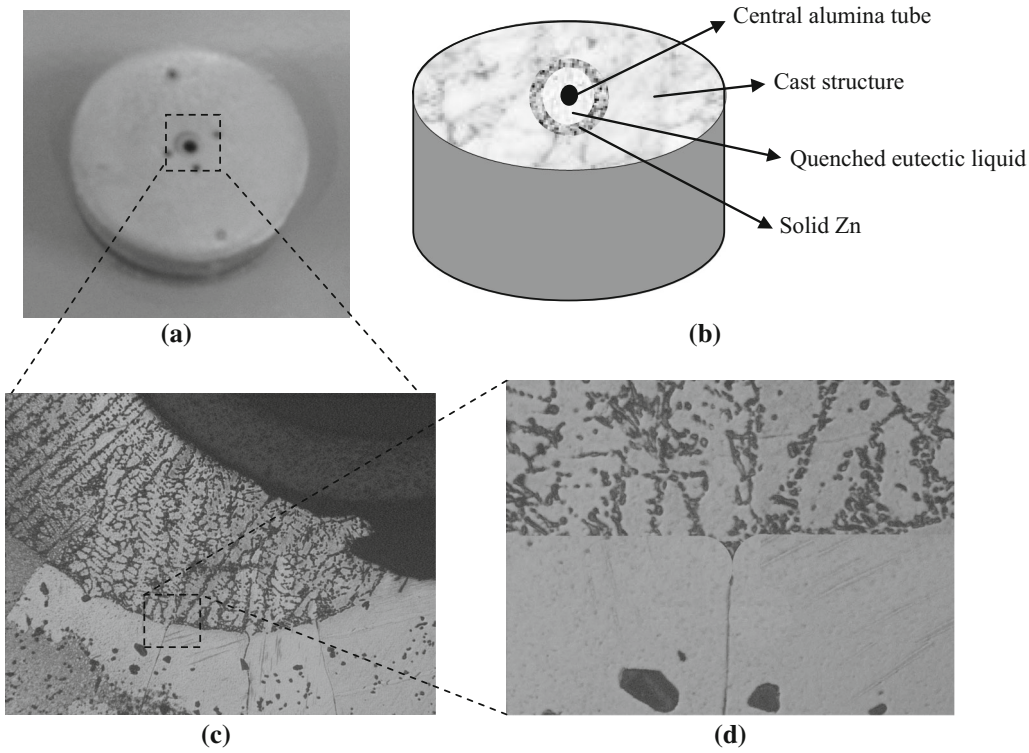

Fig. 4—(*a*) The view of the transverse section of sample. (*b*) Schematic representation of sample. (*c*) Solid–liquid interface on sample. (*d*) Typical grain boundary groove shape for solid Zn.

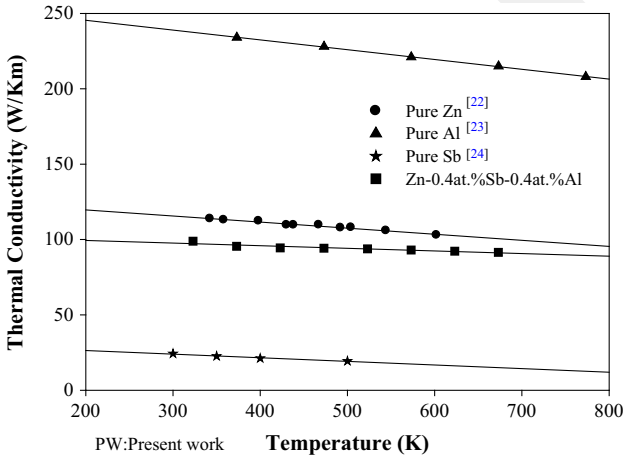

Fig. 5—Thermal conductivity of eutectic solid *vs* temperature in Zn-Al-Sb system.

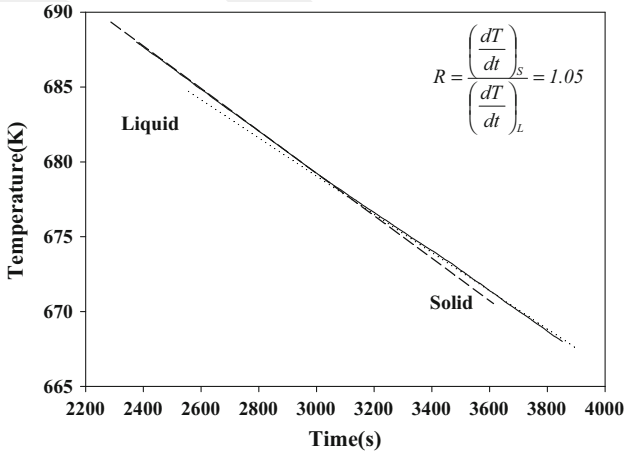

Fig. 6—The cooling rate of eutectic Zn-0.4 at. pct Al-0.4 at. pct Sb system.

since a thick liquid layer (10 mm) is required. A layer of this size would certainly have led to convection. If the thermal conductivity ratio of the liquid phase to the solid phase is known and the thermal conductivity of the solid phase is measured at the melting temperature, the thermal conductivity of the liquid phase can then be evaluated. The thermal conductivity ratio can be obtained during directional growth with a Bridgman-type growth apparatus. The details of the experimental procedure are given in References 13 through 17.

The thermal conductivity ratio of the eutectic liquid (Zn-0.4 at. pct Al-0.4 at. pct Sb) to the eutectic solid (Zn-0.4 at. pct Al-0.4 at. pct Sb), $R = K_{L(\text{eutectic})}/K_{S(\text{eutectic})}$, was measured to be 1.05, as shown in Figure 6, with a Bridgman-type growth apparatus. The thermal conductivity of the Zn-Al-Sb eutectic solid at the eutectic temperature was also measured to be 91.30 W/Km. The thermal conductivity of the eutectic liquid was then determined to be 95.87 W/Km. Thus, the thermal conductivity ratio of the equilibrated eutectic liquid phase (Zn-0.4 at. pct Al-0.4 at. pct Sb) to the solid Zn phase, $R = K_{L(\text{eutectic liquid})}/K_{S(Zn)}$, is also found to be 0.95 using the values of thermal conductivity of the eutectic liquid and thermal conductivity of the

solid Zn.[22] The thermal conductivities of the solid and liquid phases for Zn-Al-Sb eutectic solid and their ratios used in the determination of the Gibbs–Thomson coefficient are given in Table I.

A comparison of the values of K_S and K_L for the Zn-Al-Sb alloy obtained in the present work with the values of K_S and K_L for Zn-based alloys[22,25–27] obtained in previous works is also given in Table I. The values of thermal conductivities obtained in the present work are little lower than the other values of thermal conductivities for Zn-based binary and ternary alloys in Table 1. The reason for this little difference is probable for the melting temperatures of the alloys. As can be seen in Table I, there is a good compatibility between the values of the present work and previous works in the limits of experimental errors.

E. *Measurement of Temperature Gradient in the Solid Phase*

The average temperature gradient of the solid phase must be determined for each grain boundary groove shape. This was done by measuring the input power, the length of heating wire, the position of the solid–liquid interface, and the value of K_S for solid Zn phase at the eutectic point. Using these measured values in Eq. [4], the temperature gradient can be determined for each grain boundary groove shape. The total fractional uncertainty in the measurement of the temperature gradient is about 6.5 pct.[14]

III. RESULTS AND DISCUSSION

A. *Determination of Gibbs–Thomson Coefficient*

If the thermal conductivity ratio of the equilibrated liquid phase to the solid phase, the coordinates of the grain boundary groove shape, and the temperature gradient of the solid phase are known, the Gibbs–Thomson coefficient (Γ) can be obtained using the numerical method described in detail in Reference 13. The experimental error in the determination of the Gibbs–Thomson coefficient is the sum of experimental errors in the measurement of the temperature gradient, thermal conductivity, and groove coordinates. Thus the total error in the determination of the Gibbs–Thomson coefficient is estimated to be about 7 pct.[14]

The Gibbs–Thomson coefficients for solid Zn in equilibrium with the eutectic liquid (Zn-0.4 at. pct Al-0.4 at. pct Sb) were determined with the present numerical model using ten equilibrated grain boundary groove shapes. Typical grain boundary groove shapes for solid Zn in equilibrium with the eutectic liquid are shown in Figure 7.

The values of Γ for solid Zn are given in Table II. The average value of Γ from Table II is

Table I. Thermal Conductivities of Solid and Liquid Phases and their Ratios at their Eutectic Temperatures for Zn-Based Alloys

Alloy	Phases	Melting Temperature (K)	K (W/Km)	$R = K_L/K_S$
Zn-Al-Sb	eutectic liquid (Zn-0.4 at. pct Al-0.4 at. pct Sb)	678.50	95.87 ± 6.71	1.05
	eutectic solid (Zn-0.4 at. pct Al-0.4 at. pct Sb)		91.30 ± 6.39	
	eutectic liquid (Zn-0.4 at. pct Al-0.4 at. pct Sb)		95.87 ± 6.71	0.95
	solid Zn[22]		100.90 ± 7.06	
Zn-Al-Bi[25]	liquid (Zn-12.7at. pct Al-1.6 at. pctBi)	649.15	115.33 ± 8.07	0.85
	solid (Zn-3.0 at. pct Al-0.3 at. pctBi)		135.68 ± 9.50	
Zn-Cu[26]	peritectic liquid (Zn-1.8 at. pct Cu)	695.65	114.7 ± 8.03	0.81
	Zn solution (Zn-2.8 at. pct Cu)		141.6 ± 9.91	
	peritectic liquid (Zn-1.8 at. pct Cu)		114.7 ± 8.03	0.84
	ε ($CuZn_5$) phase (Zn-12 at. pct Cu)		136.3 ± 9.54	
Zn-Al[27]	liquid (Zn-11.3 at. pctAl)	653	108.6 ± 7.60	0.89
	solid (Zn-11.3 at. pctAl)		122 ± 8.54	
	liquid (Zn-11.3 at. pctAl)		108.6 ± 7.60	1.02
	Zn solid solution (Zn-2.4 at. pctAl)		106.5 ± 7.46	

$(5.4 \pm 0.4) \times 10^{-8}$ Km for solid Zn in equilibrium with the Zn-Al-Sb eutectic liquid.

B. *Determination of Entropy of Fusion Per Unit Volume*

In order to determine the solid–liquid interfacial energy, it is also necessary to know the entropy change per unit volume, ΔS^*, for solid phase. In order to determine the entropy change per unit volume, it is also necessary to know the Gibbs free energy for a two-component system.

The Gibbs free energy for a two-component system is not as simple as for one-component system; it is a function of the composition of both solid and liquid phases (Figure 8). The Gibbs free energy for a two-component system can be written as

$$G = n_A \mu_A + n_B \mu_B, \qquad [8]$$

where n_A and n_B are the number of atoms and μ_A and μ_B are the chemical potentials for components A and B, respectively. For a two-component material, the molar free energy change due to the curvature effect for a spherical incompressible solid at constant composition and temperature can be expressed as follows:

$$\left(\frac{\partial G}{\partial P}\right)_{T,n_A,n_B} = n_A \left(\frac{\partial \mu^A}{\partial P}\right)_{T,n_A,n_B} + n_B \left(\frac{\partial \mu^B}{\partial P}\right)_{T,n_A,n_B}, \qquad [9]$$

$$\left(\frac{\partial G}{\partial P}\right)_{T,n_A,n_B} = n_A V^A + n_B V^B, \qquad [10]$$

where V^A and V^B are the partial molar volumes of the components A and B, respectively. From Eq. [7], the molar free energy change can be written as

$$\Delta G = n_A \int_{P_L}^{P_S} V^A dP + n_B \int_{P_L}^{P_S} V^B dP, \qquad [11]$$

$$\Delta G = \left(n_A V^A + n_B V^B\right) \Delta P, \qquad [12]$$

$$\Delta G = V_S \Delta P. \qquad [13]$$

The pressure difference for a curved spherical interface is given by[28]

$$\Delta P = \frac{2\sigma_{SL}}{r}. \qquad [14]$$

Thus, the free energy change for an incompressible spherical solid can be written as

$$\Delta G = \frac{2\sigma_{SL}}{r} V_S. \qquad [15]$$

For a two-component system, the change in equilibrium compositions due to the curvature of the interface can be obtained from the free energy composition diagram as shown in Figure 8. This diagram is a plot of average free energy per atom $G_{S\infty}$, $G_{L\infty}$, G_{Sr} against

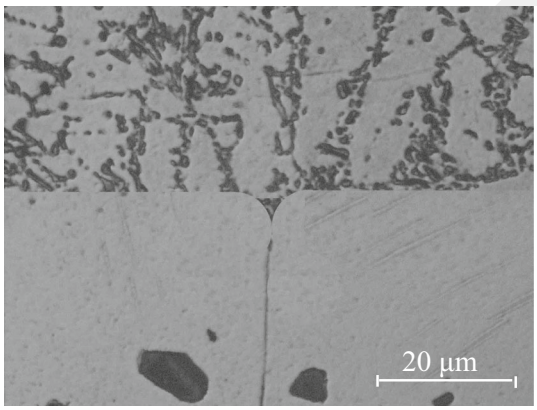

Fig. 7—Typical grain boundary groove shape for solid Zn in equilibrium with the Zn-0.4 at. pct Al-0.4 at. pct Sb eutectic liquid.

Table II. The Gibbs–Thomson Coefficients for Solid Zn in Equilibrium with the Zn-0.4 at. pct Al-0.4 at. pct Sb Eutectic Liquid

Groove No	$G_K \times 10^2$ (K/m)	$\alpha°$	$\beta°$	Gibbs–Thomson Coefficient $\Gamma_{LHS} \times 10^{-8}$ (Km)	Gibbs–Thomson Coefficient $\Gamma_{RHS} \times 10^{-8}$ (Km)
1	9.12	11.5	12.6	5.3	5.1
2	9.53	11.2	11.5	5.3	5.3
3	12.69	14.1	13.8	5.3	5.4
4	11.78	13.3	12.8	5.0	5.6
5	11.32	12.0	11.2	5.3	5.5
6	11.36	10.3	12.8	5.8	5.5
7	11.40	12.8	10.9	5.4	5.3
8	12.48	12.6	13.1	5.5	5.4
9	16.13	12.8	10.6	5.6	5.5
10	17.58	15.2	13.1	5.3	5.3
$\bar{\Gamma} = (5.4 \pm 0.4) \times 10^{-8}$ Km					

The subscripts LHS and RHS refer to left hand side and right hand side of the groove, respectively.

composition. The equilibrium condition is given by the common tangent, *i.e.,* the chemical potential must everywhere have the same value as well as the fact $T_S = T_L$ at the solid–liquid interface. As can be seen from Figure 8, the G_{Sr} curve is simply shifted upwards at constant composition to compare with the $G_{S\infty}$ free energy curve. A relation between Δg, ΔX_L, and ΔT_r can be obtained from Figure 8. From Figure 8, the change of liquid composition can be written as

$$\Delta X_L = X_{Lr} - X_{L\infty} \quad [16]$$

for small changes and assuming approximately similar triangles (DHK triangle~DEF triangle) on the free energy composition diagram as shown in Figure 8

$$\Delta\mu = \mu^B_{Sr} - \mu^B_{S\infty} = \frac{1 - X_{L\infty}}{X_{S\infty} - C_{L\infty}}\Delta G, \quad [17]$$

where μ^B_{Sr} and $\mu^B_{S\infty}$ are the chemical potentials for a curved interface and a flat interface, respectively, and $C_{L\infty}$ and $C_{S\infty}$ are the equilibrium concentrations of solid and liquid phases for a flat interface, respectively.

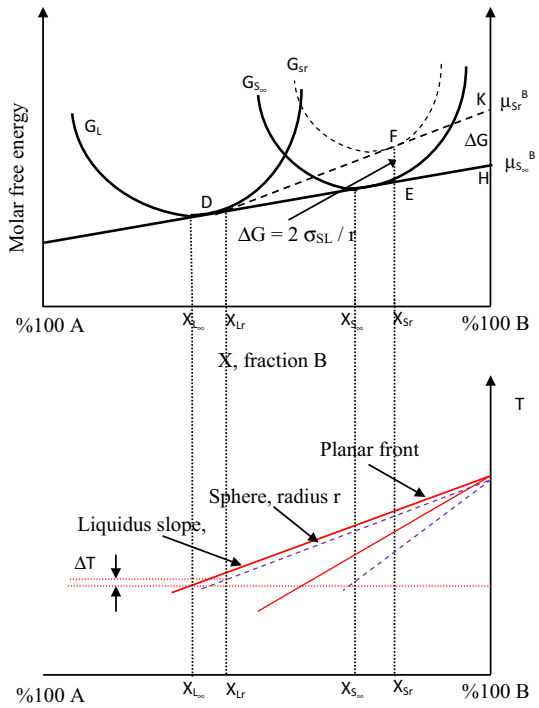

Fig. 8—The free energy composition diagram showing the effect of interface energy on the equilibrium between the solid and liquid and the change of liquidus and solidus lines for a spherical interface.

Since

$$\mu = \mu_O + R\ T\ \ln\ (a), \quad [18]$$

where a is the activity which is the product of activity coefficient and concentration, one obtains[14]

$$\Delta G = \Delta\mu = RT\ln\left(\frac{X_{Lr}}{X_{L\infty}}\right) = RT\ln\left(1 + \frac{\Delta X_L}{X_{L\infty}}\right), \quad [19]$$

where R is the gas constant, T is the equilibrating temperature, and $\Delta X_L = X_{Lr} - X_{L\infty}$. For small values of ΔX_L

$$\Delta G = \Delta\mu = R\ T\ \ln\frac{\Delta X_L}{X_{L\infty}}. \quad [20]$$

Equating Eqs. [15], [17], and [20], the change of liquid composition is obtained as

$$\Delta X_L = \left[\frac{(1 - X_{L\infty})X_{L\infty}}{(X_{S\infty} - X_{L\infty})}\right]\left(\frac{2\,\sigma_{SL}}{r\,RT}V_S\right). \quad [21]$$

The change in liquid composition due to curvature of the interface at constant temperature can be expressed as a change in temperature at constant composition using the liquidus slope, *i.e.*, $\Delta T_r = m_L\Delta X_L$ (Figure 8). Thus the curvature undercooling can be expressed as a function composition of phases, liquidus slope, equilibrium temperature, principle radius, and solid–liquid interfacial energy as follows:

$$\Delta T_r = \frac{2\sigma_{SL}\,m_L V_S}{r\,RT}\frac{(1 - X_{L\infty})\ X_{L\infty}}{(X_{S\infty} - X_{L\infty})}. \quad [22]$$

For a spherical solid–liquid interface $r_1 = r_2 = r$ and the Eq. [2] becomes

$$\Delta T_r = \frac{2\sigma_{SL}}{r\,\Delta S^*}. \quad [23]$$

Thus, the effective entropy change per unit volume, ΔS^*, for a two-component system is obtained from the Eqs. [22] and [23] as follows:

$$\Delta S^* = \frac{RT\,(X_{S\infty}\ -\ C_{L\infty})}{m_L\,(1 - C_{L\infty})C_{L\infty}}\frac{1}{V_S}. \quad [24]$$

In present work, the grain boundary groove shapes were observed in the ternary eutectic system. Thus, it was not possible to determine the value of effective

Table III. Some Physical Properties for Solid Zn in Equilibrium with Zn-0.4at. pct Al-0.4 at. pct Sb Eutectic Liquid

Alloy	Solid Phase	Liquid Phase	Eutectic Melting Point, K	ΔS^*(J K^{-1} m^{-3})
Zn-Al	Zn-2.4 at. pct Al	Zn-11.3 at. pct Al	653[27]	1.61×10^6[27]
Zn-Al-Sb	Zn	Zn-0.4 at. pct Al-0.4 at. pct Sb	678.5[19]	1.55×10^6

entropy change per unit volume for solid phase in the ternary eutectic system from the Eq. [24] For given two different temperatures T_1 and T_2 at a constant pressure, the effective entropy change per unit volume can be written as

$$\Delta S_1^* = \frac{\Delta q_1}{T_1}, \qquad [25]$$

$$\Delta S_2^* = \frac{\Delta q_2}{T_2}, \qquad [26]$$

where Δq_1 and Δq_2 are the absorbed or emitted heat at a constant temperature, respectively. If the solid phases are same and the difference between T_2 and T_1 is small, the value of Δq_1 should be close to the value of Δq_2 *i.e.,* $\Delta q_1 \approx \Delta q_2$. Dividing Eq. [26] by Eq. [25] gives

$$\Delta S_2^* = \Delta S_1^* \frac{T_1}{T_2}. \qquad [27]$$

If the value of ΔS_1^* at T_1 is known or determined for solid phase in binary eutectic system, the value of ΔS_2^* at T_2 can be then estimated from Eq. [26] using the known values of ΔS_1^*, T_1, and T_2 for the same solid phase in ternary eutectic system.

The molar volume, V_S, is expressed as

$$V_S = V_c N_a \frac{1}{n}, \qquad [28]$$

where V_c is the volume of the unit cell, N_a is the Avogadro's number, and n is the number of molecules per unit cell.

Some physical properties for solid Zn in equilibrium with Zn-0.4 at. pct Al-0.4 at. pct Sb eutectic liquid are given in Table III. The value of ΔS^* for solid Zn in the Zn-0.4 at. pct Al-0.4 at. pct Sb was determined to be 1.55×10^6 J K^{-1} m^{-3} from Eq. [27] using the relevant parameters and is also given in Table III. The error in the determination of entropy of fusion per unit volume is estimated to be about 5 pct.[13,14,29]

C. *Evaluation of the Solid–Liquid Interfacial Energy*

If the values of Γ and ΔS^* are known, the value of the solid–liquid interfacial energy, σ_{SL}, can be evaluated from Eq. [3] The solid–liquid interfacial energy of the solid Zn in equilibrium with the Zn-Al-Sb eutectic liquid (Zn-0.4 at. pct Al-0.4 at. pct Sb) was calculated to be $(83.4 \pm 10.0) \times 10^{-3}$ J m^{-2} using the values of Γ and ΔS^*. The experimental error in the determination of solid–liquid interfacial energy is the sum of experimental errors of the Gibbs–Thomson coefficient and the entropy change of fusion per unit volume. Thus, the total experimental error of the solid–liquid interfacial energy evaluation in the present work is estimated to be about 12 pct.

Table IV. A Comparison of the Values of Γ, τ, σ_{SL}, and σ_{gb} for Zn Obtained in the Present Work with the Values of Γ, τ, σ_{SL}, and σ_{gb} Obtained in Previous Works for Similar Eutectic Alloys

System	Solid Phase	Liquid Phase	Temperature (K)	Entropy of Fusion $\Delta S^* \times 10^6$ (J/K m^3)	$\Gamma \times 10^{-8}$ (Km)	$\sigma_{SL} \times 10^{-3}$ (J m^{-2})	$\sigma_{gb} \times 10^{-3}$ (J m^{-2})
Zn-Al	Zn solution (Zn-2.4 at. pctAl)[27]	Zn-11.3 at. pctAl[27]	653	1.61[27]	5.80 ± 0.18[27]	93.50 ± 8.41[27]	182.30±18.23[27]
	Zn solution (Zn-2.4 at. pctAl)[30]	Zn-11.3 at. pct Al[30]	653	1.61[27]	6.41 ± 0.51[30]	103.33 ± 13.4[30]	204.11±30.62[30]
	Zn_β solution(Al-66.5at. pctZn)[15]	Al-88.7 at. pct Zn[15]	653	3.13[15]	3.41 ± 0.14[15]	106.94 ± 9.62[15]	204.72± 22.52[15]
Zn-Bi	Zn	Zn-Bi	692			85±15[31]	
Zn-In	Zn	Zn-In	692			87±15[31]	
Zn-Sn	Zn	Zn-Sn	433			99±10[32]	
			692			90±15[31]	
Zn-Cu	ε ($CuZn_5$) (Zn-12 at. pct Cu)[26]	Zn-1.75at. pct Cu[26]	695.65	1.55[26]	4.9 ± 0.3[26]	76.0 ± 9.1[26]	150.3 ±19.5[26]
Zn-Al-Bi	Zn solution (Zn-3.0 at. pct Al-0.3 at. pctBi)[25]	Zn-12.7 at. pct Al-1.6 at. pctBi	649.15	1.57[25]	5.1 ± 0.4[25]	80.1 ± 9.6[25]	158.6 ±20.6[25]
Zn-Al-Sb[PW]	Zn	(Zn-0.4 at. pct Al-0.4 at. pct Sb)	678.5	1.55	5.4 ± 0.4	83.4 ± 10.0	138.9 ±18.1

PW: Present Work.

D. *Grain Boundary Energy*

If the grains on either side of the grain boundary are in the same phase, then the grain boundary energy can be expressed as

$$\sigma_{gb} = 2\,\sigma_{SL}\cos\theta, \quad [29]$$

where

$$\theta = \frac{\theta_A + \theta_B}{2}, \quad [30]$$

is the angle that the solid–liquid interfaces make with the y-axis. The angles, θ_A and θ_B, were obtained from the cusp coordinates, x, y, using a Taylor expansion for parts at the base of the groove. According to Eq. [29], the value of σ_{gb} should be smaller or equal to twice the solid–liquid interfacial energy, *i.e.*, $\sigma_{gb} \leq 2\sigma_{SL}$.

The value of the grain boundary energy for the solid Zn was found to be $(138.9 \pm 18.1) \times 10^{-3}$ J m^{-2} using the values of the σ_{SL} and θ in Eq. [29] The estimated error in the determination of θ angles was found to be 1 pct. Thus the total experimental error in the resulting grain boundary energy is about 13 pct.

Interfacial energy anisotropy is considered to play a critical role in many phase transformations. The determination of the effects of anisotropy on the interfacial energy is difficult. In the literature, there are no theoretical or experimental available data for the anisotropy of the interfacial energy of the solid Zn phase. Thus the solid–liquid interfacial energy is assumed to be isotropic. A comparison of the values of the Gibbs–Thomson coefficient (Γ), solid–liquid interfacial energy (σ_{SL}), and grain boundary energy (σ_{gb}) for solid Zn measured in the present work with the values of Γ, σ_{SL}, σ_{gb} for solid Zn phases in different alloy systems obtained in previous works is given in Table IV. As can be seen from Table IV, the resulting values of σ_{SL} and σ_{gb} for solid Zn in the Zn-Al-Sb system agree well with the values of σ_{SL} and σ_{gb} determined in previous works[30–32] for solid Zn phases in different systems. From the comparison, it can be concluded that for solid Zn in equilibrium with different liquid, the Gibbs–Thomson coefficient seems to be constant and does not depend on the composition of liquid, but the solid–liquid interfacial energy changes slightly with a composition of the liquid at a constant temperature.

IV. CONCLUSIONS

A radial temperature gradient on the sample was established by heating from the center with a single heating wire and cooling the outside of the sample with a heating/refrigerating circulating bath. The equilibrated grain boundary groove shapes for solid Zn in equilibrium with the Zn-Al-Sb eutectic liquid were observed from a quenched sample. Some thermo-physical properties such as the Gibbs–Thomson coefficient, solid–liquid interfacial energy, and grain boundary energy of solid Zn in equilibrium with the Zn-Al-Sb eutectic liquid were experimentally determined from the observed grain boundary groove shapes. The thermal conductivity of the eutectic solid phase at the eutectic temperature was also determined. All these determined values agree well with the values determined in previous works for solid Zn phases in different systems. In future research, the solid–liquid interfacial energy may also be theoretically determined by recently improved computational simulation methods[33,34] by applying the method to the grain boundary groove shapes.

ACKNOWLEDGEMENTS

This project was supported by Erciyes University Scientific Research Project Unit under Contract No.: FDK-2013-4467. The authors would like to thank Erciyes University's Scientific Research Project Unit for their financial support. Yemliha Altıntas would like to thank to TUBITAK for their support through a scholarship.

REFERENCES

1. N. Eustathopoulos, M.G. Nicholas, and B. Drevet: *Wettability at High Temperatures*, Pergamon Materials Series. Pergamon, Oxford, 1999.
2. J.W. Martin, R.D. Doherty, and B. Cantor: *Stability of Microstructure in Metallic Systems*, Cambridge University Press, Cambridge, 1997.
3. D. Turnbull: *J. Appl. Phys.*, 1950, vol. 21, pp. 1022–28.
4. D.R.H. Jones: *J. Mater. Sci.*, 1974, vol. 9, pp. 1–17.
5. N. Eustathopoulos: *Int. Met. Rev.*, 1983, vol. 28, pp. 189–210.
6. G.F. Bolling and W.A. Tiller: *J. Appl. Phys.*, 1960, vol. 31, pp. 1345–50.
7. G.E. Nash and M.E. Glicksman: *Philos. Mag.*, 1971, vol. 24, pp. 577–92.
8. D.R.H. Jones and G.A. Chadwick: *J. Cryst. Growth*, 1971, vol. 11, pp. 260–64.
9. R.J. Schaefer, M.E. Glicksman, and J.D. Ayers: *Philos. Mag.*, 1975, vol. 32, pp. 725–43.
10. S.C. Hardy: *Philos. Mag.*, 1977, vol. 35, pp. 471–84.
11. N.B. Singh and M.E. Glicksman: *J. Cryst. Growth*, 1989, vol. 98, pp. 573–80.
12. J.J. Hoyt, M. Asta, T. Haxhimali, A. Karma, R.E. Napolitano, and R. Trivedi: *MRS Bull.*, 2004, vol. 29, pp. 935–39.
13. M. Gündüz and J.D. Hunt: *Acta Metall.*, 1985, vol. 33, pp. 1651–72.
14. N. Maraşlı and J.D. Hunt: *Acta Mater.*, 1996, vol. 44, pp. 1085–96.
15. K. Keşlioğlu and N. Maraşlı: *Mater. Sci. Eng. A*, 2004, vol. 369, pp. 294–301.
16. Y. Ocak, S. Akbulut, K. Keşlioğlu, and N. Maraşlı: *J. Phys. D Appl.*, 2008, vol. 41, pp. 1–10.
17. Y. Ocak, S. Akbulut, K. Keşlioğlu, N. Maraşlı, E. Çadırlı, and H. Kaya: *Chin. Phys. B*, 2009, vol. 18 (9), pp. 3952–59.
18. A. Bulla, C. Carreno-Bodensiek, B. Pustal, R. Berger, A. Bührig-Polaczek, and A. Ludwig: *Metall. Mater. Trans. A*, 2007, vol. 38A, pp. 1956–64.
19. G. Klancnik: *J. Medved*, 2013, vol. 66, pp. 14–19.
20. S. Peng, J. Lu, C. Che, G. Kong, and Q. Xu: *Appl. Surf. Sci.*, 2010, vol. 256 (16), pp. 5015–20.
21. B. Zhang: *Development of corrosion resistant galvanising alloys, metallurgy and materials*, The University of Birminghman, 2005.
22. Y.S. Touloukian, R.W. Powell, C.Y. Ho, and P.G. Klemensi: *Thermal Conductivity Metallic Elements and Alloys,* vol. 1, New York, Washington, 1970, pp. 498.
23. Y.S. Touloukian, R.W. Powell, C.Y. Ho, and P.G. Klemensi: *Thermal Conductivity Metallic Elements and Alloys,* vol. 1, New York, Washington, 1970, pp. 60.
24. Y.S. Touloukian, R.W. Powell, C.Y. Ho, and P.G. Klemensi: *Thermal Conductivity Metallic Elements and Alloys,* vol. 1, New York, Washington, 1970, pp. 10–14.
25. S. Aksöz, Y. Ocak, N. Maraşlı, and K. Keşlioğlu: *Exp. Therm. Fluid Sci.*, 2011, vol. 35, pp. 395–404.

26. Y. Kaygısız, S. Akbulut, Y. Ocak, K. Keşlioğlu, N. Maraşlı, E. Çadırlı, and H. Kaya: *J. Alloy Compd.*, 2009, vol. 487, pp. 103–108.
27. K. Keşlioğlu and N. Maraşlı: *Metall. Mater. Tran. A*, 2004, vol. 35A, pp. 3665–72.
28. R. Trivedi and J.D. Hunt: in *The Mechanics of Solder Alloy: Wetting and Spreading; Surface and Interface Energy Measurement*, F.G. Yost, F. M. Hosking and Darrel R. Frear, eds., Van Nostrand Reinhold, New York, 1993, pp. 191.
29. J.W. Christian: *The Theory of Transformations in Metals and Alloys, Part I*, 2nd ed., Pergamon, Oxford, 1975.
30. U. Böyük, S. Engin, and N. Maraşlı: *J. Alloy Compd.*, 2009, vol. 476, pp. 213–19.
31. A. Passerone, R. Sangiorgi, N. Eustathopoulos, and P. Derse: *Met. Sci. Technol.*, 1979, vol. 13, pp. 359–65.
32. D. Camel, N. Eustathopoulos, and J. Desre: *Acta Met.*, 1980, vol. 28, pp. 239–47.
33. B. Li, H. Qin: *Feature-Aware Reconstruction of Volume Data Via Trivariate Splines,* Pacific Graphics Short Papers, 2011, pp. 49–54.
34. B. Li and H. Qin: *Comput. Gr.*, 2012, vol. 36, pp. 329–40.